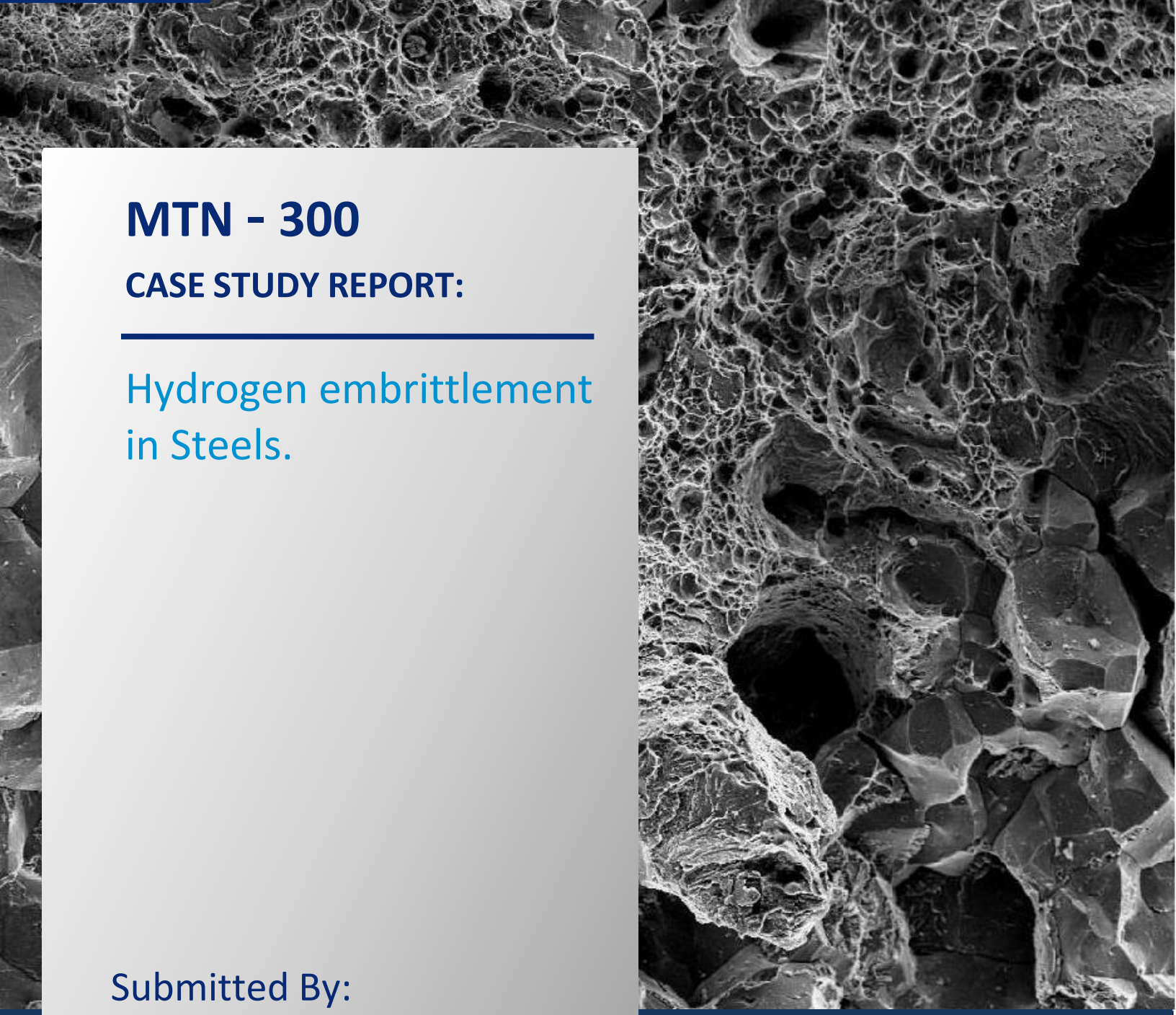

MTN - 300

CASE STUDY REPORT:

Hydrogen embrittlement in Steels.

Submitted By:

Shreyansh Tiwari (21118079)

Sudarsan R (21118086)

Under the guidance of

Prof. Anish Karmakar,

MMED , IIT - Roorkee

Table of Contents

1.Abstract:

This report investigates hydrogen embrittlement in steels, a critical issue causing material failure in high-strength alloys. Initially, the study explores theoretical aspects such as quantum mechanics and dislocation mobility affected by hydrogen, aiming to understand the underlying mechanisms that lead to structural vulnerabilities in metals.

Methodologically, the study combines discussions among material science experts with advanced experimental approaches, including micromechanical tests and spectroscopic methods. These techniques are utilized to examine the actions of hydrogen at the atomic level, particularly how it influences dislocation behavior and contributes to void formation and brittle fractures in steels.

Experimentally, the report delves into hydrogen permeation and diffusion in dual-phase (DP) and complex-phase (CP) steels using electrochemical techniques. It was discovered that CP steels exhibit higher hydrogen diffusion coefficients due to their finer microstructure and lower carbon content, which facilitates easier hydrogen movement. This section of the study also investigates hydrogen trapping mechanisms, noting that DP steels have higher trap densities, enhancing their hydrogen trapping capabilities, while CP steels show stronger trapping potential due to higher trap activation energies.

The findings highlight the critical role of microstructural features in determining steel's susceptibility to hydrogen embrittlement. This study not only deepens the understanding of the mechanisms at play but also contributes to the development of materials with enhanced resistance to hydrogen embrittlement. Future efforts should focus on optimizing steel microstructures to mitigate the risks associated with hydrogen exposure, thereby enhancing the reliability of industrial applications.

2.Introduction

Hydrogen embrittlement represents a significant challenge across various industries, notably in sectors such as oil and gas, aerospace, automotive, and infrastructure. This phenomenon occurs when hydrogen atoms infiltrate metal structures, leading to the development of microscopic cracks and, ultimately, catastrophic material failures under stress. The study of hydrogen embrittlement is crucial not only for ensuring the structural integrity and longevity of critical components but also for advancing safety standards and operational reliability in these high-stakes fields. Despite extensive research, the complex interactions between hydrogen and different metals are not fully understood, necessitating ongoing investigation to develop more effective prevention and mitigation strategies.

Economically, the implications of hydrogen embrittlement are profound, as failures related to this issue can lead to costly downtimes, repairs, and replacements, not to mention the potential for severe accidents. Industries are increasingly looking at ways to minimize risks through material selection, design modifications, and innovative treatment processes such as post-weld heat treatments and the use of coatings that inhibit hydrogen ingress. Understanding and addressing hydrogen embrittlement is not only about reducing economic losses but also about enabling the broader adoption of hydrogen as a clean energy carrier, crucial for the transition to a low-carbon economy. This underscores the importance of integrating robust materials science research with industry practices to foster safer and more sustainable industrial operations.

3.Timeline:

1966
- Pfeil observes intergranular and transgranular failures in ferritic steels during pickling, proposing hydrogen-enhanced decohesion.

1969
- Westlake notes the brittleness of hydrides and proposes a mechanism where hydrogen is attracted to a loaded crack tip, leading to hydride precipitation and crack growth.

1972
- Beachem uses carbon replica techniques to observe fracture surfaces at different stress intensity factors, challenging previous notions about hydrogen embrittlement and suggesting the term "hydrogen-assisted" cracking.

1970s
- Lynch proposes the Adsorption-Induced Dislocation Emission (AIDE) mechanism, emphasizing hydrogen's role at crack tips in facilitating dislocation emission.

1980
- Stott C Zaremba calculate the energy of inserting a hydrogen atom into a homogeneous electron gas, shedding light on hydrogen's tendency to segregate to surfaces and vacancies in metals.

1990
- The Illinois group (Birnbaum, Robertson, Sofronis) introduces the Hydrogen Enhanced Localized Plasticity (HELP) mechanism, focusing on hydrogen in solution ahead of the crack tip.

2001
- Nagumo suggests that hydrogen is attracted to vacancies, enhancing the concentration of vacancies and supporting the defactant concept.

4. Evolution of the theory

4a. Mechanisms of Hydrogen-Induced Fracture

Hydrogen-induced fracture mechanisms have been a significant focus since the latter half of the 20th century. A pivotal discovery by Westlake in 1969 revealed that hydrides, formed upon exposure to hydrogen, significantly reduced the ductility of certain metals, fundamentally altering their mechanical properties and leading to catastrophic failures. In 1972, Beachem demonstrated a shift in fracture modes based on the stress intensity experienced by a sample, challenging previous understandings of hydrogen embrittlement, and marking a shift in the theory of localized hydrogen-enhanced plasticity.

The 1970s also saw Lynch's introduction of the Adsorption-Induced Dislocation Emission (AIDE) mechanism, illustrating how hydrogen could facilitate the emission of dislocations—key agents of plastic deformation within the crystal lattice of metals. Concurrently, the Illinois group developed the Hydrogen Enhanced Local Plasticity (HELP) theory, which posited that hydrogen could promote plasticity at the crack tip, enhancing crack propagation in hydrogen-charged metals. This period marked significant advancements in understanding the complex interactions of hydrogen with metal structures.

4b. Understanding Dislocation Behavior

The Illinois group's use of transmission electron microscopy provided crucial insights into how hydrogen affects dislocation mobility in materials. Their findings indicated that hydrogen segregates to dislocations, altering their behavior and mobility. This is key in understanding how hydrogen facilitates crack initiation and propagation by modifying dislocation glide, thereby reducing the barriers to dislocation emission at crack tips. This aligns with observed reductions in elastic interactions and supports the growing body of experimental evidence that hydrogen significantly influences material mechanics at the microscopic level.

4c. Segregation and Interaction with Dislocations

Moreover, hydrogen tends to segregate to dislocations which is critically important to its embrittling effect. In 2001, Nagumo proposed that when hydrogen is attracted to vacancies within the metal's lattice, the stage is set for the formation of micro voids, a precursor to crack formation. This underscores the importance of understanding hydrogen's interaction with the microstructural features of materials. Stott C Zaremba's calculations in 1980 provided further insight into the mechanisms of hydrogen segregation. They show that hydrogen prefers to segregate to metal surfaces and vacancies, which has an impact on the emission and mobility of dislocation loops. This knowledge is crucial for developing materials and treatments that can prevent hydrogen embrittlement.

4d. Role of Interstitials and Grain Boundary Embrittlement

Unlike hydrogen, some other interstitials such as carbon and boron boost the cohesion of metals. Their ability to form covalent bonds with metal atoms contributes to material strengthening, a stark contrast to hydrogen's embrittling effect. Indeed, hydrogen-induced grain boundary embrittlement (HIGBE) has been a fruitful area of research. We now understand that HIGBE may be more akin to a "hardening" of the matrix surrounding grain boundaries as opposed to their direct embrittlement. The formation of hydrides at dislocations – contributing to crack propagation along grain boundaries – for instance, illustrates the intricate interplay between hydrogen and material microstructure. The figure set 1 explains it in detail.

Figure Set 1

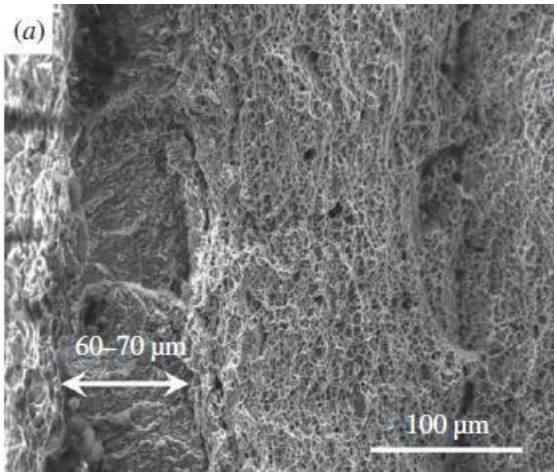

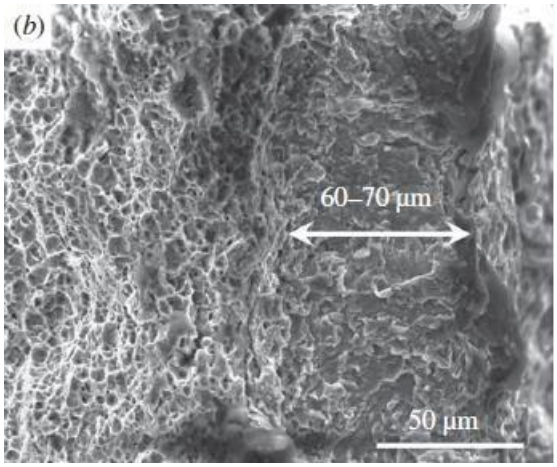

The major difference you would probably notice between the two images is the presence of hydrogen. Image (a) shows the fracture surface without hydrogen pre-charging; the material wasn't exposed to any hydrogen prior to being stretched and broken. Image (b) shows the fracture surface within situ hydrogen charging, which means that hydrogen was introduced into the material as it was being stretched. In a material that is susceptible to hydrogen embrittlement, we can expect to see lots more of so-called brittle fracture features in a photo like image (b): more jagged and uneven surfaces and many fewer or no "dimples."

5. Attributes of Hydrogen Embrittlement

5a. The Significance of Understanding Hydrogen Embrittlement Mechanisms

Understanding the mechanisms of hydrogen embrittlement is a pivotal part of progressing materials science, especially the creation of alloys that resist the effect. At its heart, this is about the crucial role of dislocation mobility. Hydrogen is particularly adept at lowering the energy needed to form kink pairs, and it is this that is the chief cause behind embrittlement. The effect is neatly explainable through both the thermodynamic and density functional theory (DFT) calculations, and it is an illustration of how the mere presence of hydrogen can change the basic physical nature of materials at a microscopic (but incredibly important) level. In a body-centered cubic (bcc) metal, this is particularly noticeable -- the softening effects of kink pair formation are much more pronounced than in face-centered cubic (face) metals due to different dislocation characteristics.

However, this is not just an area of study. This kind of understanding is vitally important for any industry that depends on safety-critical structures, including aerospace and nuclear power. The more you know about these processes, the more likely you are not only to create a predictive model for material behavior, but to meet the regulatory requirements that show a deep, fundamental knowledge of just how your materials behave under a wide variety of conditions. It lets you interpolate more cleverly between experimental results and proves to the people who write the checks that you are not blindly staking the business's future on dicey engineering solutions. In short, this does not just improve our knowledge for its own sake -- it improves the safety and reliability of critical infrastructure that modern society depends upon.

5b.The Critical Role of Vacancies in Hydrogen-Assisted Cracking

The role of vacancies in hydrogen-assisted cracking is a subject of considerable interest in materials science. Vacancies, or regions where an atom is missing from a crystal lattice, are thought to be central to the mechanisms by which micro voids associated with cracks grow in advance of material failure. The presence of hydrogen is understood to lead to enhanced levels of vacancies, which in turn increase the rate of creep at lower temperatures.

Complicating the behavior of vacancies in the presence of H is whether or not vacancies agglomerate in the presence of hydrogen; equilibrium conditions suggest that they do not, due to the loss of favorable H sites for vacancy arrays, but non-equilibrium processes, such as that initiated at an oxide or carbide interface, may lead to crack initiation. This tug of war between hydrogen and vacancies is emblematic of the broader efforts to understand damage mechanisms in hydrogen-exposed materials.

For instance, hydrogen-enhanced stress-induced vacancy formation has been identified as the operative damage mechanism in materials under stress of experiments give rise to superabundant vacancies. These and other recent insights have pointed to the significant need to appreciate better the role of vacancies in hydrogen-assisted cracking, starting with the recognition that vacancies are operable in both the initiation as well as the propagation phases of cracking. Such an understanding is critical in the development of more robust materials and processes to limit the deleterious effects of hydrogen on structural integrity. Refer Figure set 2 for more reference regarding the occurrence of Vacancies.

Dual Nature of Hydrogen

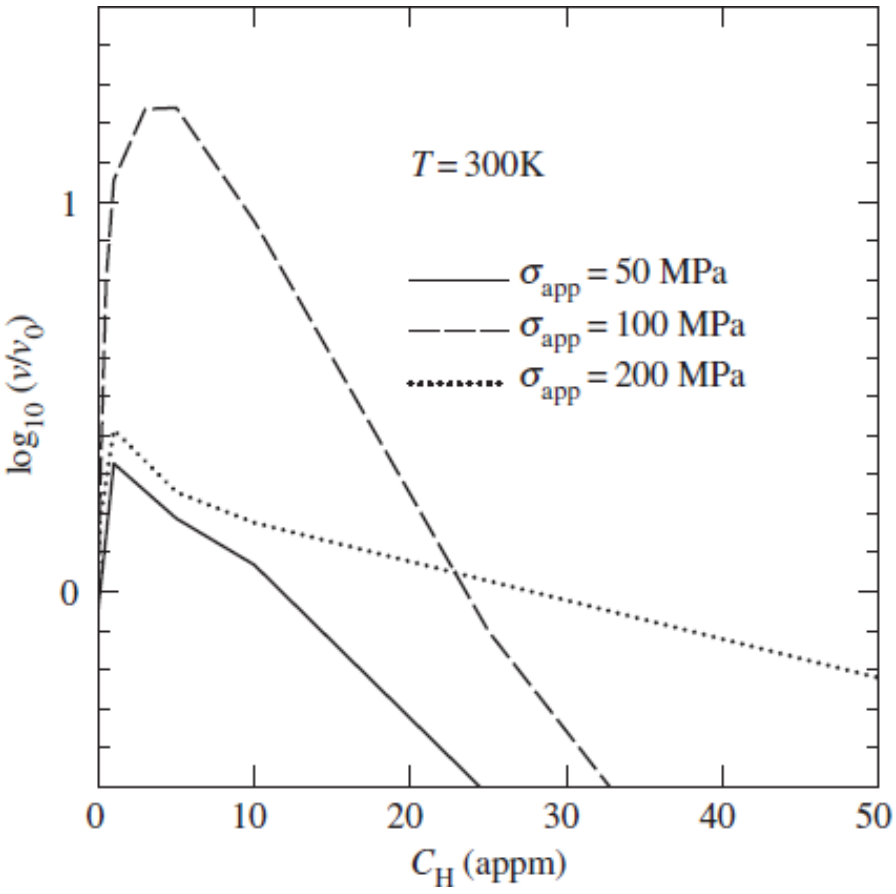

Figure set 2

As the concentration of H increases the dislocation velocity increases due to the free mobility of dislocations. But after a certain concentration it starts dropping because the impedance character of H dominates there.

Formation of Prismatic Loop :

Figure 3

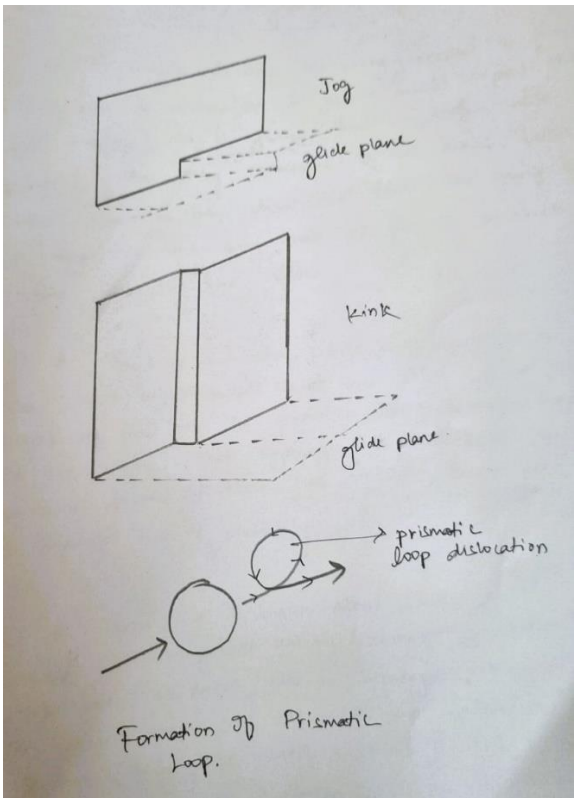

5c.DFT Study on the Interplay of Hydrogen, Vacancies, and Dislocation Dynamics in Metals

A key issue in materials science is to understand the influence of hydrogen on metals, particularly in body-centered cubic (BCC) structures, where hydrogen can affect kink pair formation and migration, the rate-limiting steps in dislocation unpinning and hence in hydrogen embrittlement. Hydrogen reduces both the formation energy of kink pairs, facilitating their production, and, through solute drag effects, can reduce kink migration along the dislocation line. These two contrasting effects can lead, under different conditions, to both increased and decreased dislocation velocities, and, hence, they have a crucial influence on the plasticity of the material.

The hydrogen also has another important effect: when a screw dislocation dissociates, the jogs on the two {110} planes generated by the splitting are free to move on

those {110} planes; in the presence of hydrogen, however, the jogs on one of the two planes, the cross-slip plane, are able to sweep out prismatic loops behind the moving dislocation, which greatly complicate the dislocation dynamics. As we show here, these, in turn, catalyze the generation of vacancies, which in this way are maintained as long-lived defects; this mechanism summarized the way in which hydrogen can perturb dislocation behaviors; it has two effects, enhancing and inhibiting dislocation motion.

5d.Exploring Carbon's Role in Hydrogen-Induced Dislocation Dynamics

Recent experiments illuminate the critical role of carbon in modulating hydrogen's impact on material properties, specifically in steel. Hydrogen was found to significantly promote dislocation nucleation and remove the upper yield stress in high-carbon steel and had a negligible effect on exceptionally low carbon steel. This suggests that there is a complex synergistic relationship between hydrogen and carbon at dislocation cores, which leads to modification of the core structure of dislocations thereby leading to increased slip. This phenomenon is echoed in other material systems, including oxygen-alloyed zirconium where hydrogen and another interstitial like oxygen act synergistically to alter dislocation behavior. This underscores the critical importance of interstitial elements, such as carbon, in dictating how susceptible materials are to hydrogen-induced changes, and the need to understand the atomic-scale interactions which give rise to these interactions, in order to ultimately be able to predict and mitigate hydrogen's effects on material integrity, at the microstructural level.

6.Introduction to Experiment

The susceptibility of AHSS to **hydrogen embrittlement (HE)** poses a significant challenge, threatening the integrity and reliability of structures made from these materials. **Hydrogen embrittlement** occurs when hydrogen atoms infiltrate the steel, migrating towards areas of high triaxial stress, potentially leading to **premature and unpredictable failures**. Such failures not only increase the risk of catastrophic incidents but also elevate maintenance and repair costs, thereby hindering the broader adoption of AHSS in critical applications.

So, understanding the behavior of hydrogen within AHSS, including its **permeation**, **solubility**, and **interaction with microstructural features**, is crucial for prevention of the risks associated with hydrogen embrittlement. One such experimental analysis is experiment based on **Electrochemical permeation.**

Electrochemical permeation studies offer a sensitive and insightful approach to analyze the diffusive flow of hydrogen through steel, and hence explaining the complex relation between hydrogen and the steel's microstructure. This study aims to research into the hydrogen permeation behavior of first-generation AHSS, specifically examining **DP** and **CP** steels, to uncover the influence of microstructure on hydrogen **diffusion**, **solubility**, and **trapping**. Through experimental analysis, this study aims to explain the mechanisms behind hydrogen behavior in AHSS, contributing to the development of steels with enhanced resistance to hydrogen embrittlement.

7.Experiment Details

Aim: To study the influence of the microstructure of DP800, DP1000 and CP1000 with respect to H permeation behavior in terms of the following:

1)Diffusion coefficient
2)The H concentration in the lattice and the traps
3)Trapping capabilities

Two DP steels with the following specifications were used:
1)DP800

tensile strength: 800MPa
thickness: 0.97 mm (average thickness)
dimensions: 30 cm*30 cm

2)DP1000
tensile strength: 1000 MPa
thickness: 0.97 mm (average thickness)
dimensions: 30 cm*30 cm

A CP steel with the following specifications:
1)CP1000
tensile strength: 1000 MPa dimensions: 30 cm*30 cm
thickness: 1.60 mm (average thickness)

Sample preparation

In order to assess the microstructure, two steel samples of dimensions 15 mm × 20 mm were prepared – one from the surface and the other from the cross- section of the prepared sample. These samples were initially ground using 4000 SiC emery paper and after that they were polished with a paste of diamond(1 μm). This process was instrumental in confirming the presence of banding patterns in the direction of rolling. The polished surfaces were then treated with

a solution of Nital(2%) for etching, after that they were examined under an SEM.

Hydrogen Permeation Cell:

In this electrochemical permeation experiment, a modified D.S. cell (the modification consists inclusion of components, namely charging and detection. These two components were separated by a test specimen, also known as working electrode)

The reduction of H+ to H takes place on one surface of the working electrode and a part of h is consumed in the material through absorption. The second surface which is exposed to the compartment is charged anodically so that H can be oxidized. The diffusion of absorbed H takes place to the other side which is further oxidized at the surface of anode to it's overpotential.

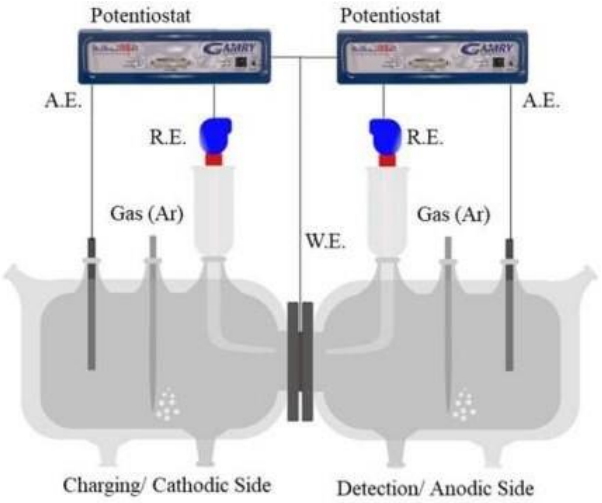

An auxiliary electrode was fixed on each compartment of the Cell. On the detection side, graphite was used while Pt mesh was used at the charging side. Also, a saturated Ag/AgCl electrode was used as a reference electrode.

Potentiostats: Two potentiostats were used whose function was as following:

- For the reduction of H+ at the cathode surface electrochemically
- For the oxidation of the Hydrogen at the side of anode

The charging was done at the surface of cathode in three steps:

Step 1(Cathodic Pre-charging):

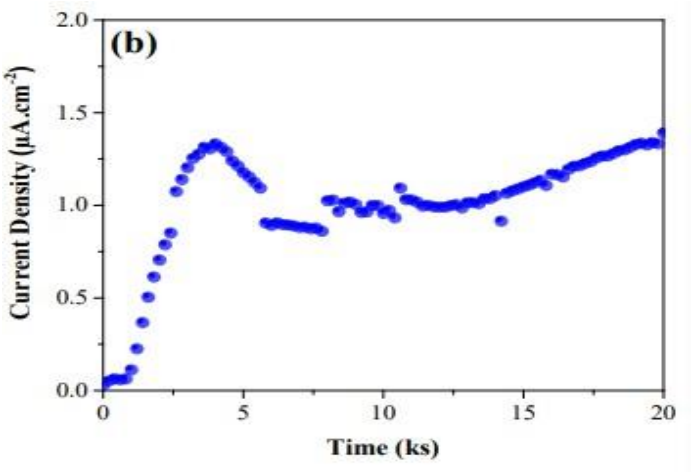

Background current density<0.3μA.cm-2
Applied cathodic current density= -10 mAcm-2(on the charging surface) Cathodic current density was applied till a steady-state current density was observed

Step 2

After the completion of previous step, the density of current on charging side was increased to the value 20-21 mA cm-2.
Again, the charging density was dropped back to -10 mA cm-2 after the density of current reached a new steady state.

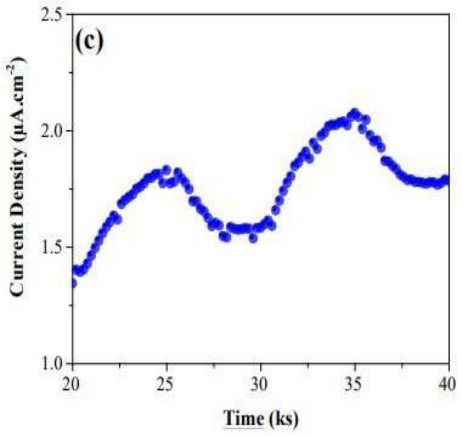

Step 3(Partial Transient Loop):
In step 3, the range of density of current which is charged was from -10mA.cm- 2 to -50 mA.cm-2. As a result, a loop is created.

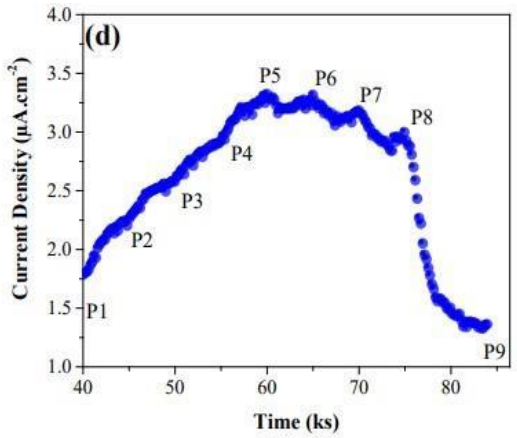

8.Results and Discussions

8a. Microstructure

The specimens were investigated under the SEM. EBSD was used to determine the phase fractions and average grain size. The below table shows the result of analysis of the phase fraction and average grain size.

Table 1: Microstructural (phase fraction, average grain size) and mechanical (tensile strength and % Elongation) features of the steels used in this study.

	Ferrite		Martensite		Bainite	U.T.S.	%Elongation
	Amount	Grain Size	Amount	Grain Size	Amount	(MPa)	
DP800	77-80%	2.10 μm	20-22%	1.32 μm	2-3%	860	29.74
DP1000	50-55%	1.34 μm	40-45%	1.29 μm	2-5%	1050	23.32
CP1000	30-35%	0.96 μm	50-55%	0.95 μm	15-20%	1024	18.04

Surface analysis

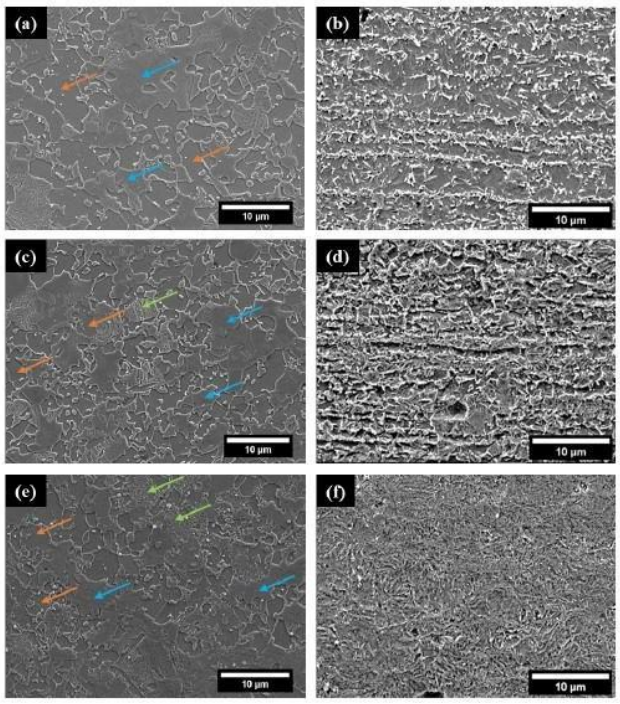

Figure 1 : Surface SEM micrographs of (a) Dual Phase 800 steel (c) Dual Phase 1000 steel and (e)Complex phase 1000 steel and cross-section SEM micrographs of (b) Dual Phase 800 (d) Dual Phase 1000 and (f) Complex Phase 1000. The orange represents ferrite, blue represents martensite and green arrows represent ferrite bainite.

Analysis of DP steels in Figure 1 (a and c) demonstrates a discontinuous ferrite matrix with embedded martensite and a minor fraction of bainite. The ferrite matrix discontinuity occurs when the martensitic phase exceeds 30%, aligning with our findings. Also, DP1000 contains a higher proportion of the martensitic phase compared to DP800, contributing to increased strength and decreased ductility. The average martensite grain size is similar for both DP800 and DP1000, resulting in a significantly larger ferrite grain size in DP800 than DP1000. CP1000 is dominated by martensite, followed by ferrite and bainite (Figure 1e). In comparison to DP steels, CP steels exhibit a notably higher bainitic phase. The average ferrite and martensite grain size in CP1000 is similar but more refined than in DP steels. The investigated steels display a retained austenite phase fraction below 0.25%. Figure 1 (panels b, d, and f) illustrates the cross-section of the examined steels (DP800, DP1000, and CP1000, respectively) along the rolling direction. Both DP800 and DP1000 exhibit a banded structure along the rolling direction and perpendicular to the hydrogen diffusion direction in this study. In contrast, the cross-section of CP1000 demonstrates a uniform distribution of phases across the cross-section.

8b. Hydrogen Diffusion Coefficient

During hydrogen charging, if the concentration of H at the charging side of the specimen reaches to a new value immediately after the cathodic current density is varied, Equation 1 & 2 can be used to determine the diffusion coefficient of hydrogen:

$$i_n = \frac{2L}{\sqrt{\pi Dt}} \sum_{n=0}^{\infty} exp\left(-\frac{(2n+1)^2 L^2}{4Dt}\right)$$

$$i_n = 1 - \frac{2L}{\sqrt{\pi Dt}} \sum_{n=0}^{\infty} exp\left(-\frac{(2n+1)^2 L^2}{4Dt}\right)$$

To determine the lattice diffusion coefficient (DL) of hydrogen, it is essential to isolate the effect of traps from the Dapp. The efficacy of traps is inversely related to the cathodic overpotential. Therefore, the apparent diffusion coefficient observed at a high applied overpotential or cathodic charging current density can be considered the lattice diffusion coefficient. The obtained DL is notably highest for CP steel, whereas the DP steels used exhibit nearly identical

DL values. Additionally, the DL surpasses the Dapp observed during pre- charging, attributed to the stabilizing surface and trap-filling effects.

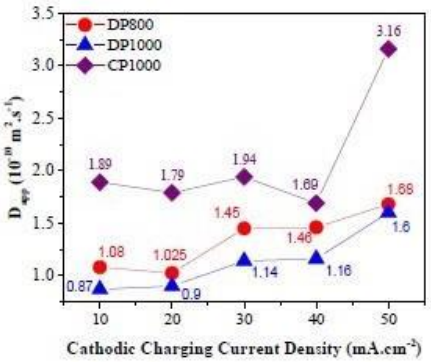

Figure 2: The change in the diffusion coefficient(apparent) of h in various given steels in this study with the variations in cathodic current density during the rise transient.

8c. Hydrogen Concentration

With knowledge of the diffusion coefficient, it becomes possible to compute, for a given steady-state, the concentration of hydrogen in the membrane at the charging side. This concentration serves as a metric for assessing the efficiency of hydrogen entry into the material. If the hydrogen concentration at the charging surface is in thermodynamic equilibrium with the sub-surface hydrogen, the total h concentration at the charging sub-surface can be defined:

$$C_T = \frac{i_{ss} * L}{F * D_{app}} \qquad \textit{Equation 3.14}$$

Similarly, the lattice hydrogen concentration (CL) can be calculated:

$$C_L = \frac{i_{ss} * L}{F * D_L} \qquad \textit{Equation 3.15}$$

Table 2: Permeability parameter values for the DP and CP steels obtained from experimental transients cathodically charged

H Charging	D_{app} (10^{-10} $m^2.s^{-1}$)			C_T ($mol.m^{-3}$)			C_L ($mol.m^{-3}$)			$C_{Trapped}$ ($mol.m^{-3}$)		
($mA.cm^{-2}$)	DP800	DP1000	CP1000	DP800	DP1000	CP1000	DP800	DP1000	CP1000	DP800	DP1000	CP1000
Precharging	1.08	0.87	1.89	1.07	1.99	0.26	0.69	1.09	0.13	0.38	0.91	0.09
-10 to -20	1.03	0.90	1.79	2.06	2.56	0.66	1.30	1.40	0.38	0.77	1.16	0.28
-20 to -30	1.45	1.14	1.94	2.37	2.77	0.91	1.56	1.55	0.53	0.81	1.22	0.38
-30 to -40	1.46	1.16	1.69	2.57	2.92	1.20	1.74	1.55	0.69	0.84	1.26	0.51
-40 to -50	1.68	1.60	3.16	2.75	3.04	1.38	1.92	1.78	0.87	0.84	1.26	0.51
-50 to -40	1.61	1.47	3.08	2.57	2.94	1.32	1.74	1.69	0.81	0.83	1.25	0.51
-40 to -30	1.60	1.32	2.55	2.34	2.81	1.22	1.53	1.57	0.73	0.82	1.23	0.49
-30 to -20	1.45	1.26	2.47	1.99	2.60	1.07	1.22	1.41	0.61	0.77	1.18	0.46
-20 to -10	1.23	1.23	2.41	1.32	2.25	1.39	0.73	1.15	0.09	0.59	1.10	0.29

The concentration of trapped h (CTrapped) at the side of the charging side is detailed in table 2 and illustrated in Figure 3 against the charging current density. Across all examined steels, CT increases with a rise in the density of charging current, reaching a saturation point at higher charging current densities (Figure 3a). This behavior is attributed to the surface coverage by adsorbed hydrogen, limiting the availability of adsorption sites for further adsorption. DP1000 exhibits the highest total hydrogen concentration at the charging surface, followed by DP800 and CP1000. Similar to the total hydrogen concentration, CL also increases with higher charging current densities, as depicted in Figure 3b. The lattice hydrogen concentration in DP steels surpasses that in CP steel. Within the DP steels, DP1000 initially exhibits a higher lattice hydrogen concentration than DP 800 at lesser current densities(charging).

However, at higher current densities, DP800 surpasses DP1000 in lattice hydrogen concentration. The concentration of trapped hydrogen (CTrapped) saturates swiftly with increasing charging current density, as shown in Figure 3.8c.

This rapid saturation is attributed to the limited number of trap sites compared to lattice sites, resulting in a quick and saturated filling of trap sites in contrast to lattice sites. Consistent with CT, CTrapped is highest for DP1000, followed by DP800 and CP1000. This observation aligns with the notion that higher charging current density minimizes the influence of traps on hydrogen diffusion, as established in previous analyses.

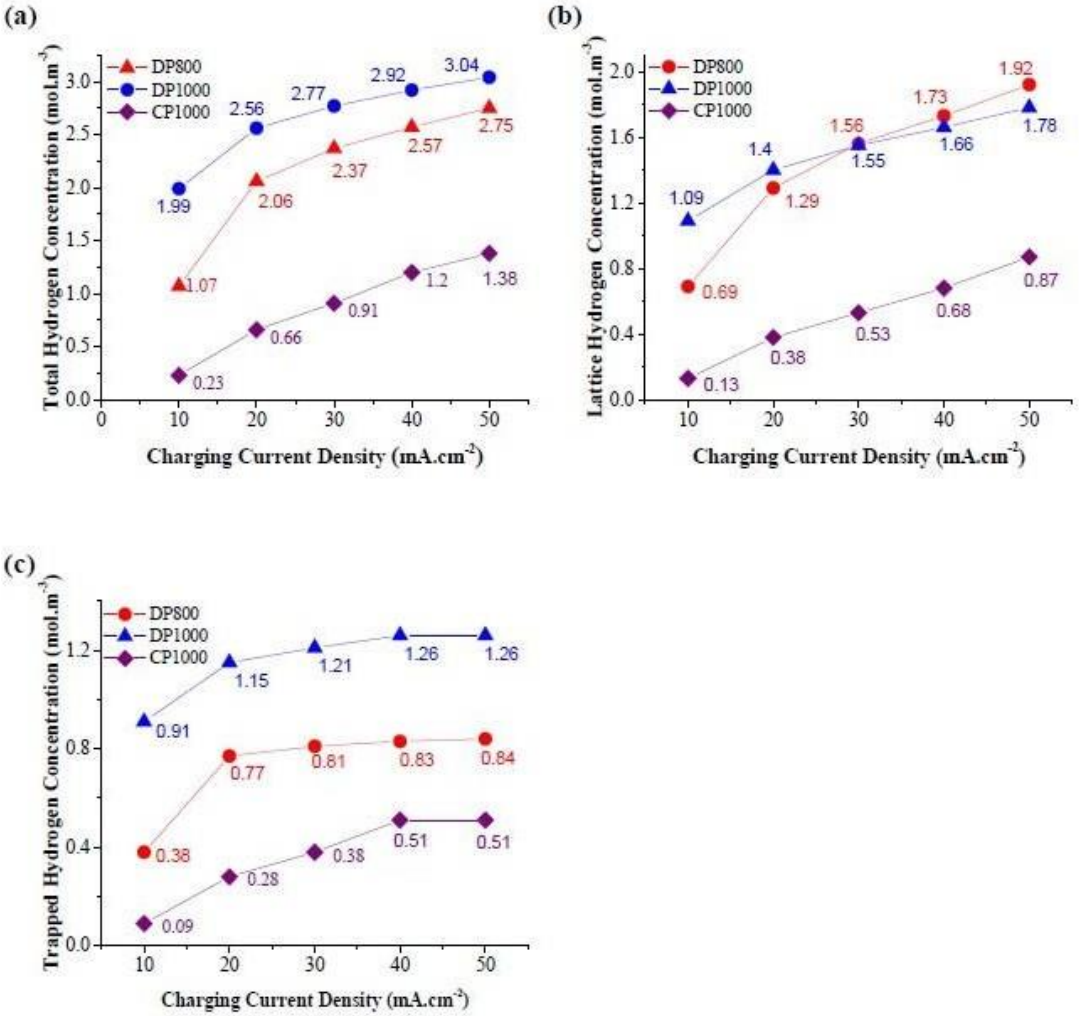

8d. Hydrogen Trapping

The permeation fall transient curve serves as a sensitive indicator of hydrogen detrapping from traps. The region beneath the curve obtained through experiment represents hydrogen which was desorbed from both lattice sites and traps, denoted as CT*

in Table 3. In contrast, the theoretical curve, fitted using DL , represents a defect-free membrane and corresponds to hydrogen desorbed solely through lattice sites. Consequently, the disparity in the area between the two curves signifies the hydrogen released from reversible trap sites.

Subsequently, the reversible trap density can be calculated using below equation. Assuming that (a) there are similar traps present and (b) each one of the trapping site can accommodate one hydrogen atom, the number of trapping sites present can be determined by the following equation:

$$N_T = \frac{2A\,X\,i_n\,X\,6.24\,X\,10^{12}}{L} \qquad \textit{Equation 3.16}$$

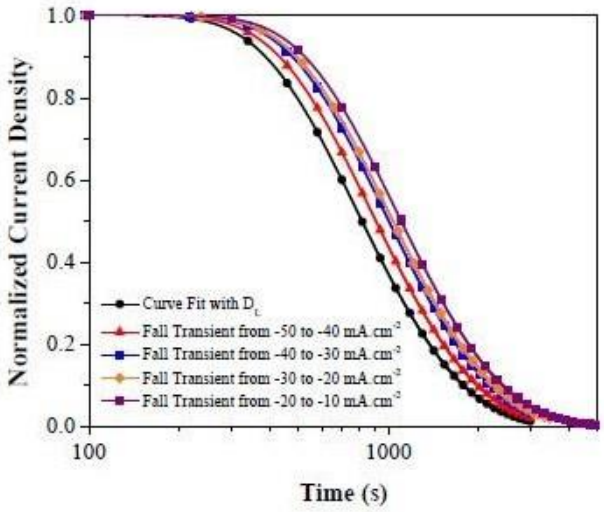

Figure 4: The schematic normalized current density for the decay transient for each fall transient

The trap density emptied during fall transients exhibits an increasing trend as the densities of the current which are charged decreases. For instance, in the case of DP800, when the density of current charged decreased from -50 to -55 mA cm^{-2} to -40 mA.cm^{-2}, the emptied reversible trap density was 7.76 x 10^{15} sites.cm^{-3}, representing approximately 12.5% of the entire number of hydrogen released from the traps. Conversely, with a further reduction in the current that was charged from -21 mA cm^{-2} to -10.1 mA cm^{-2}, the emptied trap density increased to 2.85 x 10^{16} sites.cm^{-3}, constituting about 46.2% of the total hydrogen released from reversible traps. This behavior was consistent across all investigated steels, indicating a diminishing influence of traps at higher overpotential. The calculated trap density was maximum in case of DP800, after that it was followed by DP1000 and at the end CP1000. This observation explains the steel-specific variations in trap behavior, with DP800 exhibiting the highest or maximum susceptibility to trap effects, followed by DP1000 and CP1000.

8e. Activation Energy(Ea) Calculation

The binding energy of h with trapping has a crucial part in shaping the behavior(diffusion) of hydrogen within the material. The determination of binding energy for traps can be achieved through analysis of the obtained permeation data. Let's assume that each trap accommodates one atom of hydrogen, Calculation of the binding energy of reversible traps can be done by:

$$ln\left(\frac{D_L}{D_{app}}-1\right)=ln\frac{N_T}{N_L}+\frac{E_a}{RT}$$

This equation can also be written as:

$$E_a=RT\{ln\left(\frac{D_L}{D_{app}}-1\right)-ln\frac{N_T}{N_L}\}$$

Table 3: The density of traps , total amount of hydrogen released, and the energy of activation of the specimens obtained from the fall transient of the permeation curve.

H Charging	N_t (10^{15} site.cm^{-3})			$C_{T'}$ (mol.m^{-3})			$C_{T'}/C_T$ X 100 %			E_a (kJ.mol^{-1})		
(mA.cm^{-2})	DP800	DP1000	CP1000	DP800	DP1000	CP1000	DP800	DP1000	CP1000	DP800	DP1000	CP1000
-50 to -40	7.76	1.59	0.86	0.073	0.032	0.017	40.00	33.44	32.66			
-40 to -30	8.62	3.72	1.48	0.084	0.044	0.029	37.77	32.18	28.52			
-30 to -20	16.80	10.04	2.21	0.136	0.067	0.043	37.25	32.40	28.21	34.05	37.62	38.94
-20 to -10	28.50	24.10	23.2	0.217	0.127	0.212	32.45	36.99	31.22			

References:

- Study of Diffusible Behavior of Hydrogen in First Generation Advanced High Strength Steels (Research paper by Dwaipayan Mallick , Nicolas Mary , V.S. Raja and Bernard Normand)

- Mechanisms of hydrogen embrittlement in steels: discussion.Phil. Trans. R. Soc. A 375:20170032.[http://dx.doi.org/10.1098/rsta.2017.0032]

- A study of internal hydrogen embrittlement of steels by G.P. Tiwari , A. Bose, J.K. Chakravartty , S.L. Wadekar , M.K. Totlani ,R.N. Arya , R.K. Fotedar